ISSN 1392-1207. MECHANIKA. Vol. 29, No. 6, 2023: 518–529

Kinematics and Workspace Analysis of 5-DOF Hybrid Redundantly Driven Mechanism

Qisheng ZHANG*, Ruiqin LI, Wei YAO***, Jingjing LIANG****, Feng Ping NING*****

**School of Mechanical Engineering, North University of China, Taiyuan 030051, China,*
E-mail: zhangqisheng_qs @nuc.edu.cn
***School of Mechanical Engineering, North University of China, Taiyuan 030051, China,*
E-mail: liruiqin@nuc.edu.cn (Corresponding Author)
****North of England Robotic Innovation Centre, University of Salford. Manchester M6 6AP, UK,*
E-mail: w.yao@salford.ac.uk
*****School of Mechanical Engineering, North University of China, Taiyuan 030051, China,*
E-mail: ning_fengping@163.com
*****School of Mechanical Engineering, North University of China, Taiyuan 030051, China,*
E-mail: 944719179@qq.com

https://doi.org/10.5755/j02.mech.33599

1. Introduction

Generally speaking, servo motors are often used to drive parallel mechanism (PM for short), but the emergence of hybrid-driven mechanism breaks this convention. Hybrid-driven mechanism is a multi-DOFs mechanism jointly controlled by constant velocity (CV for short) motor (uncontrollable) and servo motor (real-time controllable). The CV motor provides main power, and the servo motor bear smaller power. Originally it was proposed by Tokuz [1] of the University of Liver-pool in 1992, which has the characteristics of both traditional mechanism and controllable mechanism. By controlling the output of servo motor to accurately compensate the motion trajectory of the mechanism, high motion accuracy can be achieved. Hybrid-driven mechanism is an important branch of mechanisms and also a research hotspot of mechanisms [2]. However, during the research and development of hybrid-driven mechanism for more than 20 years, its mechanism has always been limited to the range of planar five-bar mechanism, six-bar mechanism, seven-bar mechanism and nine-bar mechanism.

The research on hybrid-driven five-bar mechanism is the most extensive and mature, due to its advantages of few bars and easy control. The research on hybrid-driven mechanism covers configuration synthesis, kinematic analysis, dynamic analysis, control methods and applications [3-12]. It is mainly used to press [5-9], walking mechanism [10], excavator [11], etc.

Redundantly actuated PM is a PM with more input components than the number of DOFs of output components [12-14]. The redundantly actuated method can eliminate the singularity of the PM and increase the workspace, which is beneficial to improve the stiffness, dexterity, positioning accuracy, obstacle avoidance performance, force transmission characteristics and reasonable load distribution of the PM [15-17]. Redundantly actuated PM has aroused the research interest of scholars because of its unique advantages. Different configurations of redundantly actuated parallel robot have been proposed and have been applied to parallel machine tool [18, 19], medical rehabilitation [20], seismic simulation instrument [21] and other fields.

Wu et al. [17] proposed a redundantly actuated U-3PSS solar tracker based on PM. Compared with non-redundantly driven U-2PSS solar tracker, U-3PSS solar tracker has larger workspace and less energy consumption in one year. Lamber et al. [18] proposed a 7-DOF PM, which not only provides 6-DOF operation, but also provides 1-DOF grasping. Because a configurable platform is used, all actuators are located on the base, which replaces the single rigid body usually used as the end effector in traditional PM. Zhang et al. [19] proposed a redundantly actuated 2RPU-2SPR PM. Aiming at the mathematical problem of forward kinematics of parallel robot, three back propagation (BP) neural network optimization strategies are used to solve it. The BP neural network with position compensation is a suitable method to solve the forward kinematics. The mechanism can be used for five-axis hybrid machine tools and is suitable for machining large heterogeneous and complex structural parts in the field of aerospace.

Wang et al. [20] proposed an ankle rehabilitation robot, which can realize three rotation movements in three directions. The rotation center of the mechanism can match the rotation axis of the ankle joint. The proposed mechanism can ensure that the redundantly actuated PM has no singularity, better dexterity and stiffness in the specified workspace. Zhao et al. [21] presented a 3-DOF redundantly actuated seismic simulation shaking table, which has strong bearing capacity and driving capacity and can resist the destructive force of earthquake.

The configurations of hybrid-driven mechanism reported in the literature are mostly multi-DOF planar linkage mechanisms. It will have a wider application prospect to introduce this hybrid-driven mechanism with high power and greater flexibility into the field of spatial mechanisms. The technical bottleneck restricting the further development of this kind of mechanism to spatial configuration is that there is no suitable configuration to satisfy the motion characteristics of hybrid-driven, that is, to solve the "controllability problem" of CV motor. By combining with other types of spatial mechanisms, it has become an idea to "copy" the relevant performance of hybrid-driven mechanism to this kind of mechanism to form a new mechanism with both characteristics.

A new type of hybrid redundantly driven mechanism (HRDM for short) integrating redundantly actuated

PM and hybrid-driven mechanism will give full play to their respective advantages. Zhang et al. [22] proposed a kind of HRDM. The basic idea of this mechanism is: HRDM with *n*-DOF is composed of N symmetrically distributed driving limb with 6-DOF that do not restrict the DOF of the mechanism and an intermediate limb that restricts the DOF of the mechanism. The intermediate limb is driven by both CV motor and servo motor, which is called hybrid redundantly actuated limb (HRDL for short).

The 3-PSS/7R HRDM proposed in reference [23] can only achieve two translation movements and one rotation movement, and its application range is limited. The movement characteristics of HRDM are periodic, flexible and controllable, which is especially suitable for the field of ankle rehabilitation. Ankle rehabilitation generally requires two rotation DOFs.

The paper is organized as follows. The configuration of a 5-DOF (5-SPS)+5R2U HRDM is constructed and the driving selection is described in Section 2. The kinematic model of the HRDM is established in Section 3. The factors affecting workspace are analyzed in Section 4. Followed by Section 5 the workspace atlas of the mechanism under different orientation angles is obtained. The output characteristics of the HRDM are analyzed in Section 6 to verify the correctness of the kinematics equations and the controllability of the mechanism. Conclusions are drawn in Section 7.

2. Configuration of the (5-SPS)+5R2U HRDM

Three-dimensional model and structure diagram of (5-SPS)+5R2U HRDM with five DOFs are shown in Figs. 1 and 2, respectively. The mechanism is composed of a moving platform, a static platform, five SPS (*S* is spherical pair, *P* is prismatic pair) limbs with the same structure and one 5R2U intermediate limb. Five SPS limbs are symmetrically distributed at the center points of the static platform and the moving platform. The intermediate limb 5R2U (Five revolute pairs and two Hooke joints) connects the static platform and the moving platform, and the center point is connected. The intermediate limb is composed of a planar five-bar mechanism and a 2U link, which is driven by both CV motor and servo motor. It is called hybrid redundantly driven limb (HRDL for short).

Link $l_1 = \overline{CD}$ is driven by an uncontrollable CV motor, and the angle between the driving link and the static platform is q_1; Link $l_4 = \overline{FG}$ is driven by a controllable servo motor, the angle between the driving link l_4 and the static platform is q_4. Through cooperative control of the driving displacement of the prismatic pairs in the 5-SPS limbs and the driving angular displacement of the HRDL's servo motor, the position and orientation of the moving platform can be controlled in real time. Among them, 5-SPS do not restrict the movement of the moving platform of the mechanism, and the DOF of the mechanism is determined by HRDL, which restricts the DOF of the moving platform to rotate around the O_2 normal of the center of the moving platform, thus the mechanism has five DOFs (three translation movements and two rotation movements). There are 7 drives of this mechanism and only 5 corresponding DOFs, thus the drives are redundant. Six of them are real-time controllable servo motors and one is uncontrollable CV motor. Therefore, the mechanism has the characteristics of hybrid-driven mechanism and redundantly actuated PM at the same time. It is an integrated mechanism of the two types of mechanisms, and has some common characteristics of the two types of mechanisms.

In Fig. 2, $l_2 = \overline{DE}$, $l_3 = \overline{FE}$, $l_5 = \overline{GO_1}$, $l_6 = \overline{O_1C}$, $l_7 = \overline{EO_2}$. The static coordinate system and the moving coordinate system are established on the (5-SPS)+5R2U HRDM static platform and the moving platform, respectively. The static coordinate system O_1-$X_1Y_1Z_1$ is fixedly connected to the static platform. The origin O_1 of the static coordinate system is located at the center of the static platform. X_1 axis points to the right through B_1, Y_1 axis is vertical and upward. Z_1 axis is determined according to the right-hand criterion.

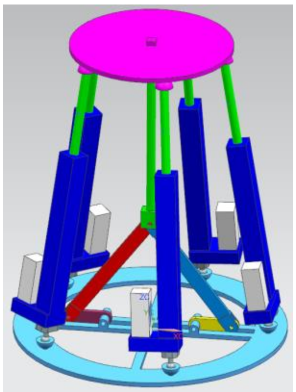

Fig. 1 3D model of (5-SPS)+5R2U HRDM

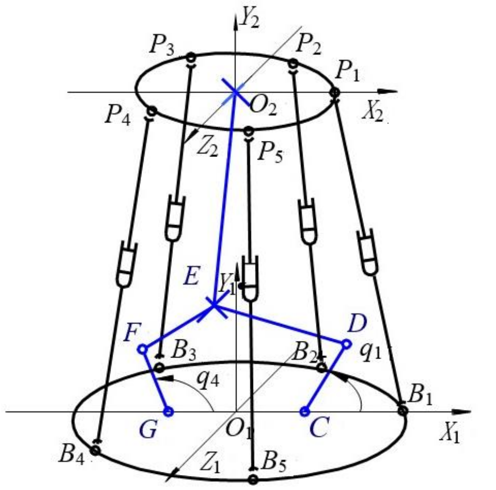

Fig. 2 Structure diagram of (5-SPS)+5R2U HRDM

The moving coordinate system O_2-$X_2Y_2Z_2$ is fixedly connected to the moving platform, and the origin O_2 of the moving coordinate system is at the center of the moving platform. In the initial orientation, X_2 axis and Y_2 axis are parallel to X_1 axis and Y_1 axis, respectively and in the same direction. $P_i\ (i = 1, 2, \cdots, 5)$ are evenly distributed on the circumference of the moving platform with radius *r*. B_i (i = 1, 2,…,5) are evenly distributed on the circumference of the static platform with radius *R*.

3. Kinematic analysis of HRDM

The position inverse solution of the (5-SPS)+5R2U HRDM is known the position and orientation

$\boldsymbol{X} = [x, y, z, \beta, \gamma]^{\mathrm{T}}$ of the moving platform and the angular displacement q_1 of the CV motor to obtain the displacement l_i ($i = 1, 2, \ldots, 5$) of the five prismatic pairs and the driving angular displacement q_4 of the servo motor of HRDL. Because the position vector equations of symmetrical 5-SPS limbs and HRDL are different, they need to be solved, separately.

3.1. Inverse position solution of HRDM

3.1.1. Inverse solution of HRDL

The orientation $\boldsymbol{X}$ of HRDM moving platform is determined by HRDL, so it is necessary to determine the orientation transformation matrix of the mechanism first. HRDL consists of a parallel 2-DOFs planar parallel mechanism ***CDEFG*** and spatial link EO_2 in series. The PM is driven by a CV motor to drive link l_1 and a servo motor to drive link l_4. Their motions are coupled at point E.

Hooke hinge is regarded as revolute pairs of two axes intersecting perpendicularly, then the CV drive limb ***CDEO₂*** can be regarded as a series mechanism, which connect to each link by revolute pairs. The link coordinate systems are established on sub-limb $CDEO_2$, as shown in Fig. 3. Z axis of coordinate system {1}-{6} corresponds to the axis of each revolute pair member, and the axis of revolute pair of coordinate system {6} is recombined with axis Z_2 of moving coordinate system O_2-$X_2Y_2Z_2$. The relative orientation of each link is described using Denavit-Hartenber parameter method. The D-H parameters of the HRDL limb $CDEO_2$ are obtained, as shown in Table 1.

Table 1

D-H parameters of the HRDL limb

No.	a_i, mm	α_{i-1}, °	d_i, mm	θ_i, °
0	l_6	0	0	0°
1	l_1	0	0	θ_1
2	l_2	0	0	θ_2
3	0	90°	0	θ_3
4	l_7	0	0	θ_4
5	0	90°	0	θ_5
6	0	0	0	θ_6
O_2	0	0	0	0

where: a_i-- The length of the connecting rod; α_{i-1}-- Torsion angle; d_i--Deviating from the displacement; θ_i-- Rotation angle.

The homogeneous transformation matrix from the linkage coordinate system {i-1} to the coordinate system {i} is ${}^{i}_{i\text{-}1}\boldsymbol{T}$, then the general expression of ${}^{i}_{i\text{-}1}\boldsymbol{T}$ is:

$$ {}^{i\text{-}1}_{i}\boldsymbol{T} = \begin{bmatrix} Q_i & [a_i] \\ 0 & 1 \end{bmatrix}, \tag{1} $$

where: $Q_i = \begin{bmatrix} c\theta_i & -s\theta_i c\alpha_i & s\theta_i s\alpha_i \\ s\theta_i & c\theta_i c\alpha_i & -s\alpha_i \\ 0 & s\alpha_i & c\alpha_i \end{bmatrix}$ $[a_i] = \begin{bmatrix} a_i c\theta_i \\ a_i s\theta_i \\ 0 \end{bmatrix}$; $\boldsymbol{Q_i}$ and $\boldsymbol{a_i}$ respectively represent the rotation of the coordinate system attached to the i_th link to the matrix consistent with the direction of the coordinate system of the (i+1)_th link and the position vector relative to the moving platform.

Orientation transformation matrix of the moving platform and static platform of the HRDM.

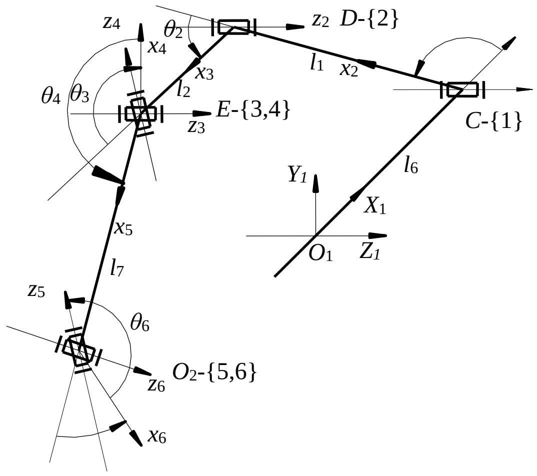

Fig. 3 The link coordinate systems of $CDEO_2$ limb

$$ {}^{O_2}_{O_1}\boldsymbol{T} = {}^{0}_{O_1}\boldsymbol{T}\,{}^{1}_{0}\boldsymbol{T}\,{}^{2}_{1}\boldsymbol{T}\cdots{}^{O_2}_{6}\boldsymbol{T} = \begin{bmatrix} m_x & n_x & o_x & p_x \\ m_y & n_y & o_y & p_y \\ m_z & n_z & o_z & p_z \\ 0 & 0 & 0 & 1 \end{bmatrix}. \tag{2} $$

According to the output motion characteristics of HRDM, the orientation transformation matrix of the static platform and the moving platform of the mechanism is obtained by Euler method $Z_\alpha Y_\beta X_\gamma$ as follows.

$$ {}^{o_1}_{o_2}\boldsymbol{T} = \begin{bmatrix} c\alpha & \text{-}s\alpha c\gamma & s\alpha s\gamma & x \\ s\alpha & c\alpha c\gamma & -c\alpha s\gamma & y \\ 0 & s\gamma & c\gamma & z \\ 0 & 0 & 0 & 1 \end{bmatrix}. \tag{3} $$

Eqs. (2) and (3) of HRDM orientation matrix are equivalent, and get:

$$ \begin{cases} x = l_7 c\theta_{1,2,3} c\theta_4 + l_2 c\theta_{1,2} + l_1 c\theta_1 + l_5 \\ y = -l_7 s\theta_4 \\ z = l_7 s\theta_{1,2,3} c\theta_4 + l_2 s\theta_{1,2} + l_1 s\theta_1 \\ \theta_{4,5} = -\pi / 2 \\ \alpha = \theta_{1,2,3} \\ \beta = 0° \\ \gamma = \theta_6 \end{cases}, \tag{4} $$

where: $\theta_{1,2,\ldots,k} = \theta_1 + \theta_2 + \ldots + \theta_k$ ($k \in N$); θ_1 = Const. The sign s stands for *sin* and c stands for *cos*.

Let the coordinate vector of point E be $\boldsymbol{X}_e = [x_e, y_e]^{\mathrm{T}}$, which is denoted by vector $\boldsymbol{r_e} = \boldsymbol{x_e} + \boldsymbol{y_e}$. Under the coupling action of limbs CDE and EFG, the position vector $\boldsymbol{r_e}$ of coupling point E changes from time to time. The HRDL can be equivalent to virtual motion limb PUU, as shown in Fig. 4. The dual drivers are arranged at the two driving revolute pairs C and G of the plane 5R mechanism to drive q_1 and q_4 respectively. The servo motor accurately compensates the trajectory of point E. The CV motor drives the CD link, and the servo motor drives the FG link. Driven by the two driving links, the driven links DE and EF are driven to make the E point output flexible track. Therefore, the CDE sub-limb meets the kinematic constraints of $CDEFG$ PM at the same time. The included angle between the links $l_i(i = 1, 2, 3, 4)$ and the horizontal axis is $q_i(i = 1, 2, 3, 4)$, where $q_i = \theta_i$, $(i = 1, 2)$.

Using closed vector method, the vector equations of servo motor driving limb and CV motor driving limb are established, respectively.

$$\boldsymbol{O_1E} = \boldsymbol{O_1C} + \boldsymbol{CD} + \boldsymbol{DE}, \tag{5}$$

$$\boldsymbol{O_1E} = \boldsymbol{O_1G} + \boldsymbol{GF} + \boldsymbol{FE}. \tag{6}$$

Eqs. (5) and (6) are projected to X_1 axis and Y_1 axis, respectively. Using the trigonometric equation, get:

$$\begin{cases} x_e = l_5 + l_1 c q_1 + l_2 c q_{1,2} \\ y_e = l_1 s q_1 + l_2 s q_{1,2} \end{cases}, \tag{7}$$

$$\begin{cases} x_e = -l_5 + l_4 c q_4 + l_3 c q_{3,4} \\ y_e = l_4 s q_4 + l_3 s q_{3,4} \end{cases}. \tag{8}$$

According to the assembly relation of the five-bar mechanism in the workspace, and y_e is located above $X_1O_1Z_1$ plane.

$$\begin{matrix} |\boldsymbol{FG} - \boldsymbol{EF}| \le |\boldsymbol{O_1E}| \le |\boldsymbol{FG} + \boldsymbol{EF}| \\ |\boldsymbol{CD} - \boldsymbol{DE}| \le |\boldsymbol{O_1E}| \le |\boldsymbol{CD} + \boldsymbol{DE}| \end{matrix}. \tag{9}$$

Solving Eq. (9), the inverse solution is obtained as folows:

$$\begin{cases} \begin{cases} q_1(X) = at\left(\dfrac{z_e}{x_e - l_6}\right) - at\dfrac{l_2 s(q_2)}{l_1 + l_2 c(q_2)} & (10.1) \\ q_2(X) = at\dfrac{\pm\sqrt{1-F^2}}{F} & (10.2) \end{cases} \\ \begin{cases} q_3(X) = at\dfrac{\pm\sqrt{1-G^2}}{G} & (10.3) \\ q_4(X) = at\left(\dfrac{z_e}{x_e + l_6}\right) - at\dfrac{l_3 s(q_3)}{l_4 + l_3 c(q_3)} & (10.4) \end{cases} \end{cases}, \tag{10}$$

where:

$$F = \frac{(x_e - l_6)^2 + z_e^2 - l_1^2 - l_2^2}{2l_1l_2}, G = \frac{(x_e - l_5)^2 + z_e^2 - l_3^2 - l_4^2}{2l_3l_4}.$$

The *sign* at stands for *arctan*.

Because link CD is driven by CV motor which can only move in one direction, after the trajectory planning is completed, the angle q_1 is determined at any given time. Therefore, when the position and orientation is given, the angle of transition from l_1 to l_2 is also determined according to Eq. (10.2). Due to the existence of CV motor, not all trajectories $\boldsymbol{X}$ of HRDM in the workspace can be realized, and the inverse solution does not exist everywhere in the same configuration. For the planned trajectory, if the initial configuration of HRDL is determined, q_{30} will be determined accordingly, assuming that it meets the function determined by $q_3(\mathbf{X})$.

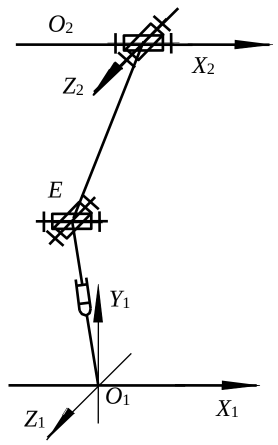

Fig. 4 Equivalent diagram of HRDL

Similarly, the initial angles q_{10} and q_{40} are determined. For a planned trajectory $\boldsymbol{X}$, once the initial configuration of HRDL is determined, although q_4 and q_3 have two solutions, in order to ensure the continuity of the trajectory, q and q_3 can only be the trajectory on the function of the law determined by $q_3(\mathbf{X})$ and $q_4(\mathbf{X})$, otherwise q_4 and q_3 will have a great jump, and the mechanism cannot have controlled. Therefore, with the determination of the initial configuration of HRDL, the operation law of q_4 and q_3 will also be determined. The $q_1(i = 1, 2, 3, 4)$ of whole limbs is unique. Eq. (10) is the inverse solution of the HRDL.

The coordinates of point E can be obtained by homogeneous transformation.

$${}^3_O\boldsymbol{T} = \left({}^0_O\boldsymbol{T}\,{}^1_0\boldsymbol{T}\,{}^2_1\boldsymbol{T}\,{}^3_2\boldsymbol{T}\right) = {}^{O'}_O\boldsymbol{T}\left({}^4_3\boldsymbol{T}\,{}^5_4\boldsymbol{T}\,{}^6_5\boldsymbol{T}\,{}^{O'}_6\boldsymbol{T}\right)^{-1} = \\ = \begin{bmatrix} {}^3m_x & {}^3n_x & {}^3o_x & {}^3p_x \\ {}^3m_y & {}^3n_y & {}^3o_y & {}^3p_y \\ {}^3m_z & {}^3n_z & {}^3o_z & {}^3p_z \\ 0 & 0 & 0 & 1 \end{bmatrix}. \tag{11}$$

From Eq. (5), get:

$$x_e = {}^3p_x = f(\boldsymbol{X}),\ y_e = {}^3p_y = g(\boldsymbol{X}),\ z = \ p = 0.$$

Point E of the HRDL is the coupling point driven by constant velocity motor and servo motor. When the equivalent virtual link is in different orientation X, the vector $\boldsymbol{r}_e = \boldsymbol{O_1E}$ is different, and its length equivalent to the virtual link length $\boldsymbol{l}_v = |\boldsymbol{r_e}|$ is also variable. The inverse solution of the general equation is transformed into solution $\boldsymbol{l}_v$.

After the position vector of coupling point E is determined, the orientation of the HRDL can be finally determined.

$$\boldsymbol{l}_v = \boldsymbol{x}_e + \boldsymbol{z}_e, \tag{12}$$

$$\boldsymbol{l}_v = \sqrt{x_e^2 + z_e^2}. \tag{13}$$

3.1.2. Inverse solution of 5-SPS limbs

According to the size parameters of the mechanism, get $\boldsymbol{B_i} = \mathrm{Rot}(Z, \pi(i-1)/5)\begin{bmatrix} R & 0 & 0 \end{bmatrix}, \quad (i = 1, 2, \cdots, 5)$. the coordinate vectors in static coordinates $\boldsymbol{B_i} = \begin{bmatrix} B_{ix}, B_{iy}, B_{iz} \end{bmatrix}^{\mathrm{T}} \ (i = 1, 2, \cdots, 5)$.

The coordinate vector ${}^{O_2}\boldsymbol{P_i} = \begin{bmatrix} {}^{O_2}P_{ix}, {}^{O_2}P_{iy}, {}^{O_2}P_{iz} \end{bmatrix}^{\mathrm{T}}$ $(i = 1, 2, \cdots, 5)$ connected with the center point ${}^{O_2}\boldsymbol{P_i} = \mathrm{Rot}(Z, \pi(i-1)/5)\begin{bmatrix} r & 0 & 0 \end{bmatrix}$ of the spherical pairs in the moving coordinate system is represented as the coordinate vector $\boldsymbol{P_i} = \begin{bmatrix} P_{ix}, P_{iy}, P_{iz} \end{bmatrix}^{\mathrm{T}}$ in the static coordinate system.

$$\boldsymbol{P_i} = \begin{bmatrix} P_{ix}, P_{iy}, P_{iz} \end{bmatrix}^{\mathrm{T}} = \boldsymbol{R}\, {}^{O_2}\boldsymbol{P}_i + \boldsymbol{P}\left(i = 1, 2, \cdots, 5\right), \qquad (14)$$

where: $\boldsymbol{R}$ denotes Euler transformation matrix represented by Z-Y-X. $\boldsymbol{P}$ denotes the coordinates of the origin of the moving coordinate system relative to the static coordinate system $\{O_1\}$.

The position vector of the five prismatic pairs in the static coordinate system is:

$$\boldsymbol{L_i} = \boldsymbol{B_i P_i} = \boldsymbol{O_1 B_i} - \boldsymbol{O_1 P_i}\left(i = 1,2,\ldots,5\right). \qquad (15)$$

Substituting the coordinates of each axis component of Eq. (15) and $\boldsymbol{B}_i$ into Eq. (16), the length of each driving link can be expressed as:

$$\boldsymbol{L_i} = \sqrt{\left(B_{ix} - P_{ix}\right)^2 + \left(B_{iy} - P_{iy}\right)^2 + \left(B_{iz} - P_{iz}\right)^2}, \quad \left(i = 1, 2, \ldots, 5\right). \qquad (16)$$

Eq. (16) is the position inverse solution model of 5-SPS limbs.

3.2. Velocity analysis of (5-SPS)+5R2U HRDM

3.2.1. Velocity analysis of HRDL

The HRDL motion input is q_1 driven by CV motor and q_4 driven by servo motor, and the motion output $\dot{\boldsymbol{l}}_v = \dot{\boldsymbol{x}}_e + \dot{\boldsymbol{y}}_e$ is generated at the coupling point E, which is the vector sum of the speeds in X_1 axis and Y_1 axis directions, and is coupled by $\boldsymbol{q}_1$ and $\boldsymbol{q}_4$. The virtual link O_1E is expressed as $\dot{\boldsymbol{l}}_v = \dot{\boldsymbol{r}}_e = \begin{bmatrix} \dot{\boldsymbol{x}}_e & \dot{\boldsymbol{y}}_e \end{bmatrix}^{\mathrm{T}}$, and the corresponding motion mapping relationship is:

$$\left(\dot{\boldsymbol{q}}_1, \dot{\boldsymbol{q}}_4\right)^{\mathrm{T}} = {}^1_1\boldsymbol{J} \cdot \dot{\boldsymbol{l}}_v, \qquad (17)$$

where: ${}^1_1\boldsymbol{J} = \mathrm{s}\left(q_2 - q_3\right)$

$$\begin{bmatrix} -l_1 \mathrm{s}q_1 \mathrm{s}\left(q_2 - q_3\right) + l_1 \mathrm{s}q_2 \mathrm{s}\left(q_1 - q_3\right) & -l_4 \mathrm{s}q_2 \mathrm{s}\left(q_4 - q_3\right) \\ l_1 \mathrm{c}q_1 \mathrm{s}\left(q_2 - q_3\right) - l_1 \mathrm{c}q_2 \mathrm{s}\left(q_1 - q_3\right) & l_4 \mathrm{c}q_2 \mathrm{s}\left(q_4 - q_3\right) \end{bmatrix}^{-1} = \begin{bmatrix} {}^1_1\boldsymbol{j}_{11} & {}^1_1\boldsymbol{j}_{12} \\ {}^1_1\boldsymbol{j}_{21} & {}^1_1\boldsymbol{j}_{22} \end{bmatrix}.$$

The velocity mapping relationship between the spatial link and the moving platform is:

$$\dot{\boldsymbol{l}}_v = {}^1_2\boldsymbol{J}\dot{\boldsymbol{X}}, \qquad (18)$$

where: ${}^1_2\boldsymbol{J} = \begin{bmatrix} {}^1_2\boldsymbol{J}_1 \\ {}^1_2\boldsymbol{J}_2 \end{bmatrix}$, ${}^1_2\boldsymbol{J}_1 = \dfrac{\partial \mathbf{l_v}}{\partial \mathbf{x_e}} \dfrac{\partial \mathbf{x_e}}{\partial \mathbf{X}}$, ${}^1_2\boldsymbol{J}_2 = \dfrac{\partial \mathbf{l_v}}{\partial \mathbf{y_e}} \dfrac{\partial \mathbf{y_e}}{\partial \mathbf{X}}$.

$${}^1\boldsymbol{J} = {}^1_1\boldsymbol{J} \cdot {}^1_2\boldsymbol{J}. \qquad (19)$$

The driving angular velocity $\dot{q}_1$ of HRDL CV motor, the driving angular velocity $\dot{q}_4$ of servo motor and the central motion output velocity $\dot{\boldsymbol{X}}$ of the moving platform are obtained from Eq. (18), Eq. (19) and Eq. (20), which satisfy the following equations:

$$\left(\dot{\boldsymbol{q}}_1, \dot{\boldsymbol{q}}_4\right)^{\mathrm{T}} = {}^1\boldsymbol{J}\dot{\boldsymbol{X}}. \qquad (20)$$

3.2.2. Velocity mapping of 5-SPS limbs

Fig. 5 shows the velocity diagram of HRDM in working state. The meaning of the symbol is expressed as follows. ${}^{O_1}\boldsymbol{V}_{O_2}$ is the velocity of the center point of the moving platform. ${}^{O_1}\boldsymbol{\omega}_{O_2}$ is the angular velocity of the center point of the moving platform. ${}^{O_1}\boldsymbol{V}_{P_i}$ is the velocity of the spherical pairs center $\boldsymbol{P}_i$. $\dot{\boldsymbol{L}}_i$ is the variation velocity of prismatic pairs of the SPS limb. ${}^{O_1}\boldsymbol{r}_{P_i}$ is the vector diameter of spherical pairs point P_i relative to the center point $\boldsymbol{O}_2$ of the moving platform. ${}^{O_1}\boldsymbol{n}_i$ is the unit direction vector of the rod L_i, then the velocity. ${}^{O_1}\boldsymbol{V}_{P_i}$ of the point P_i can be expressed as:

$${}^{O_1}\boldsymbol{V}_{P_i} = {}^{O_1}\boldsymbol{V}_{O_2} + {}^{O_1}\boldsymbol{\omega}_{O_2} \times {}^{O_1}\boldsymbol{r}_{P_i}. \qquad (21)$$

The driving velocity of the prismatic pairs $\dot{\boldsymbol{L}}_i$ on the 5-SPS limb can be expressed as the projection of ${}^{O_1}\boldsymbol{V}_{P_i}$ on L_i:

$$\dot{\boldsymbol{L}}_i = {}^{O_1}\boldsymbol{V}_{P_i}\, {}^{O_1}\boldsymbol{n}_i. \qquad (22)$$

Substituting Eq. (21) into Eq. (22), we obtain:

$$\dot{\boldsymbol{L}}_i = \begin{bmatrix} {}^{O_1}\boldsymbol{n}_i^T & \left({}^{O_1}\boldsymbol{r}_{P_i} \times {}^{O_1}\boldsymbol{n}_i\right)^T \end{bmatrix} \begin{bmatrix} {}^{O_1}\boldsymbol{V}_{O_2} \\ {}^{O_1}\boldsymbol{\omega}_{O_2} \end{bmatrix}. \qquad (23)$$

For all 5-SPS drive links, there is a velocity relationship:

$$\dot{\boldsymbol{L}} = {}^2_1\boldsymbol{J}_{O_1} \begin{bmatrix} {}^{O_1}\boldsymbol{V}_{O_2} \\ {}^{O_1}\boldsymbol{\omega}_{O_2} \end{bmatrix}, \qquad (24)$$

where: $\dot{\boldsymbol{L}} = \begin{bmatrix} \dot{\boldsymbol{L}}_1 & \dot{\boldsymbol{L}}_2 & \dot{\boldsymbol{L}}_3 & \dot{\boldsymbol{L}}_4 & \dot{\boldsymbol{L}}_5 \end{bmatrix}^{\mathrm{T}}$; .

$$
{}_{1}^{2}\boldsymbol{J}_{O_1} = \begin{bmatrix} {}^{O_1}\boldsymbol{n}_1^{\mathrm{T}} & \left({}^{O_1}\boldsymbol{r}_{P_1} \times {}^{O_1}\boldsymbol{n}_1\right)^{\mathrm{T}} \\ {}^{O_1}\boldsymbol{n}_2^{\mathrm{T}} & \left({}^{O_1}\boldsymbol{r}_{P_2} \times {}^{O_1}\boldsymbol{n}_2\right)^{\mathrm{T}} \\ {}^{O_1}\boldsymbol{n}_3^{\mathrm{T}} & \left({}^{O_1}\boldsymbol{r}_{P_3} \times {}^{O_1}\boldsymbol{n}_3\right)^{\mathrm{T}} \\ {}^{O_1}\boldsymbol{n}_4^{\mathrm{T}} & \left({}^{O_1}\boldsymbol{r}_{P_4} \times {}^{O_1}\boldsymbol{n}_4\right)^{\mathrm{T}} \\ {}^{O_1}\boldsymbol{n}_5^{\mathrm{T}} & \left({}^{O_1}\boldsymbol{r}_{P_5} \times {}^{O_1}\boldsymbol{n}_5\right)^{\mathrm{T}} \end{bmatrix}_{5\times 6}
$$

, where ${}_{1}^{2}\boldsymbol{J}_{O_1}$ is PS driving velocity mapping matrix.

When $Z_\alpha - Y_\beta - X_\gamma$ is used to represent the orientation and orientation of the moving platform, the derivative of Euler angle (α, β, γ) to time is $\dot{\alpha}$ on Z axis, $\dot{\beta}$ on the Y' axis, $\dot{\gamma}$ on the X'' axis, and $\dot{\alpha}, \dot{\beta}, \dot{\gamma}$ is non orthogonal. When the generalized angular velocity $\dot{\alpha}, \dot{\beta}, \dot{\gamma}$ is converted to the static coordinate system $\{O_1\}$, the rotational angular velocity of the moving platform is expressed by the derivative of Euler angle.

$$
\boldsymbol{\omega}_{O_2} = \begin{bmatrix} 0 & c\alpha \\ 0 & s\alpha \\ 1 & 0 \end{bmatrix} \begin{bmatrix} \dot{\alpha} \\ \dot{\gamma} \end{bmatrix}. \tag{25}
$$

The six-dimensional velocity of the moving platform is expressed as:

$$
\dot{\boldsymbol{X}} = \begin{bmatrix} \boldsymbol{v}_{O_2} & \omega_{O_2} \end{bmatrix}^{\mathrm{T}} = \begin{bmatrix} \dot{x} & \dot{y} & \dot{z} & \dot{\alpha} & \dot{\gamma} \end{bmatrix}^{\mathrm{T}}
$$

$$
\begin{bmatrix} \boldsymbol{V}_{O_2} \\ \boldsymbol{\omega}_{O_2} \end{bmatrix} = {}_{2}^{2}\boldsymbol{J}_{O_1}\dot{\mathbf{X}}, \tag{26}
$$

where: ${}_{2}^{2}\boldsymbol{J}_{O_1} = \begin{bmatrix} 1 & 0 & 0 & 0 & 0 \\ 0 & 1 & 0 & 0 & 0 \\ 0 & 0 & 1 & 0 & 0 \\ 0 & 0 & 0 & 0 & c\alpha \\ 0 & 0 & 0 & 1 & 0 \\ 0 & 0 & 0 & 0 & s\alpha \end{bmatrix}_{6\times 5}$.

Substituting Eq. (26) into Eq. (24), yield:

$$
\begin{bmatrix} \boldsymbol{V}_{O_2} \\ \boldsymbol{\omega}_{O_2} \end{bmatrix} \begin{bmatrix} \dot{\boldsymbol{L}}_1 \\ \dot{\boldsymbol{L}}_2 \\ \dot{\boldsymbol{L}}_3 \\ \dot{\boldsymbol{L}}_4 \\ \dot{\boldsymbol{L}}_5 \end{bmatrix} = {}^{2}\boldsymbol{J} \begin{bmatrix} \dot{\boldsymbol{x}} \\ \dot{\boldsymbol{y}} \\ \dot{\boldsymbol{z}} \\ \dot{\boldsymbol{\alpha}} \\ \dot{\boldsymbol{\gamma}} \end{bmatrix} = {}_{2}^{2}\boldsymbol{J}_{O_1}\dot{\mathbf{X}}, \tag{27}
$$

where: ${}^{2}\boldsymbol{J}_{5\times 5} = {}_{1}^{2}\boldsymbol{J}_{O_1}\,{}_{2}^{2}\boldsymbol{J}_{O_1} \in R^{5\times 5}$; ${}^{2}\boldsymbol{J}_{5\times 5}$ is the velocity transfer matrix in the form of Euler angular velocity.

The driving velocity of 5-SPS can be obtained by using Eq. (27).

From Eq. (20), Eq. (24) and Eq. (27), the overall Jacobian matrix of (5-SPS)+5R2U HRDM is:

$$
\boldsymbol{J} = \begin{bmatrix} {}^{1}\boldsymbol{J} \\ {}^{2}\boldsymbol{J} \end{bmatrix}. \tag{28}
$$

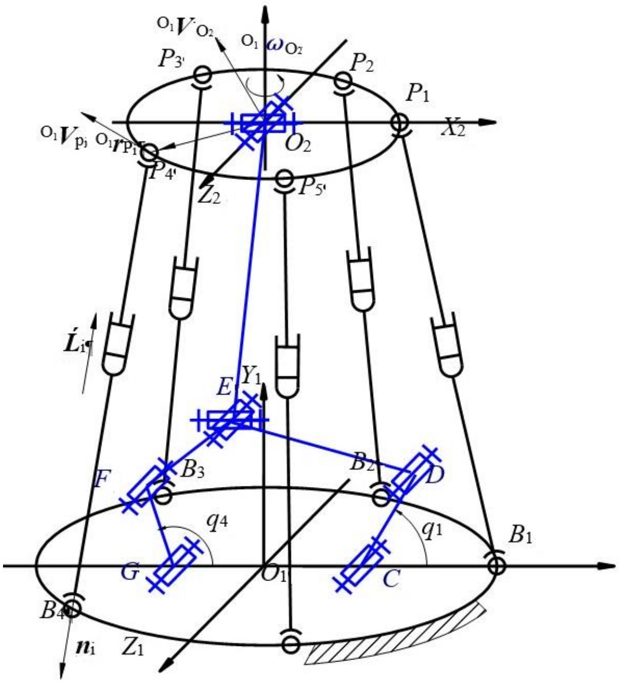

Fig. 5 Velocity analysis diagram of (5-SPS)+5R2U HRDM

3.3. Acceleration analysis of (5-SPS)+5R2U HRDM

Let $\ddot{L}_i\left(i = 1, 2, \cdots, 5\right)$ is the acceleration along L_i, then the linear acceleration $\boldsymbol{a}$ and angular acceleration ε corresponding to the moving platform are expressed as:

$$
\boldsymbol{a} = \begin{bmatrix} a_x & a_y & a_z \end{bmatrix}^{\mathrm{T}} \text{ and } \boldsymbol{\varepsilon} = \begin{bmatrix} \varepsilon_x & \varepsilon_y & \varepsilon_z \end{bmatrix}^{\mathrm{T}}.
$$

And the acceleration is calculated for the HRDL and 5-SPS limbs, respectively.

3.3.1. Acceleration analysis of HRDL

The derivative of Eq. (20) with respect to time, and obtain:

$$
\left(\ddot{\boldsymbol{q}}_1, \ddot{\boldsymbol{q}}_4\right)^{\mathrm{T}} = {}^{1}\dot{\boldsymbol{J}}\dot{\boldsymbol{X}} + {}^{1}\boldsymbol{J}\ddot{\boldsymbol{X}}. \tag{29}
$$

According to Eq. (19), ${}^{1}\dot{\boldsymbol{J}}$ can be further obtained.

$$
{}^{1}\dot{\boldsymbol{J}} = {}_{1}^{1}\dot{\boldsymbol{J}} \cdot {}_{2}^{1}\boldsymbol{J} + {}_{1}^{1}\boldsymbol{J} \cdot {}_{2}^{1}\dot{\boldsymbol{J}}. \tag{30}
$$

Next, solving ${}_{1}^{1}\dot{\boldsymbol{J}}$ and ${}_{2}^{1}\dot{\boldsymbol{J}}$, respectively

$$
{}_{1}^{1}\dot{\boldsymbol{J}} = \begin{bmatrix} {}_{1}^{1}\dot{\boldsymbol{j}}_{11} & {}_{1}^{1}\dot{\boldsymbol{j}}_{12} \\ {}_{1}^{1}\dot{\boldsymbol{j}}_{21} & {}_{1}^{1}\dot{\boldsymbol{j}}_{22} \end{bmatrix},
$$

where ${}_{1}^{1}\dot{\boldsymbol{j}}_{ij} = \dfrac{\partial \dot{\boldsymbol{j}}_{ij}}{\partial Q}\dfrac{\partial Q}{\partial X}$, $\boldsymbol{Q} = \begin{bmatrix} q_1 & q_2 & q_3 & q_4 \end{bmatrix}$.

Further calculation, the expression of ${}_{2}^{1}\dot{\boldsymbol{J}}$ can be expressed as follows:

$$
\dot{\boldsymbol{J}} = \begin{bmatrix} \dot{\boldsymbol{J}} \\ \dot{\boldsymbol{J}} \end{bmatrix}, \tag{31}
$$

where:

$$ {}_{2}^{1}\dot{\boldsymbol{J}} = \frac{\partial^2 x_e}{\partial \mathbf{X}^2} = \begin{bmatrix} \frac{\partial^2 x_e}{\partial x \partial \mathbf{X}} & \frac{\partial^2 x_e}{\partial y \partial \mathbf{X}} & \frac{\partial^2 x_e}{\partial z \partial \mathbf{X}} & \frac{\partial^2 x_e}{\partial \alpha \partial \mathbf{X}} & \frac{\partial^2 x_e}{\partial \gamma \partial \mathbf{X}} \end{bmatrix}; $$

$$ \dot{\boldsymbol{j}} = \frac{\partial y}{\partial \mathbf{X}} = \begin{bmatrix} \frac{\partial y}{\partial x \partial \mathbf{X}} & \frac{\partial y}{\partial y \partial \mathbf{X}} & \frac{\partial y}{\partial z \partial \mathbf{X}} & \frac{\partial y}{\partial \alpha \partial \mathbf{X}} & \frac{\partial y}{\partial \gamma \partial \mathbf{X}} \end{bmatrix}. $$

3.3.2 Acceleration analysis of 5-SPS

The derivative of Eq. (24) with respect to time, and obtain:

$$ \ddot{\boldsymbol{L}} = \begin{bmatrix} \boldsymbol{n} & (\boldsymbol{r} \times \boldsymbol{n}) \end{bmatrix} \mathbf{A} \begin{bmatrix} \boldsymbol{V} \\ \boldsymbol{\omega} \end{bmatrix} + \begin{bmatrix} \boldsymbol{V} & \boldsymbol{\omega} \end{bmatrix} \boldsymbol{h} \begin{bmatrix} \boldsymbol{V} \\ \boldsymbol{\omega} \end{bmatrix}, \tag{32} $$

where: $\mathbf{A} = \begin{bmatrix} \boldsymbol{a} & \boldsymbol{\varepsilon} \end{bmatrix}^{\mathrm{T}}$,

$$ \boldsymbol{h}_i = \frac{1}{\boldsymbol{L}_i} \begin{bmatrix} -{}^{O_1}\hat{\boldsymbol{n}}_i^2 & {}^{O_1}\hat{\boldsymbol{n}}_i^2 \, {}^{O_1}\hat{\boldsymbol{r}}_{p_i} \\ -{}^{O_1}\hat{\boldsymbol{r}}_{p_i} \, {}^{O_1}\hat{\boldsymbol{n}}_i^2 & L_i \, {}^{O_1}\hat{\boldsymbol{r}}_{p_i} \, {}^{O_1}\hat{\boldsymbol{n}}_i^2 + {}^{O_1}\hat{\boldsymbol{r}}_{p_i} \, {}^{O_1}\hat{\boldsymbol{n}}_i^2 \, {}^{O_1}\hat{\boldsymbol{r}}_{p_i} \end{bmatrix}_{6\times 6}. $$

The derivative of Eq. (26) with respect to time, and obtained:

$$ \boldsymbol{A} = {}_{2}^{2}\boldsymbol{J}_{O_1} \ddot{\mathbf{X}} + \boldsymbol{v}_p^T \boldsymbol{H} \boldsymbol{v}_p, \tag{33} $$

where: $\boldsymbol{H} = \begin{bmatrix} \boldsymbol{H}_1 & \boldsymbol{H}_2 & \boldsymbol{H}_3 & \boldsymbol{H}_4 & \boldsymbol{H}_5 & \boldsymbol{H}_6 \end{bmatrix}^{\mathrm{T}}$;

$$ \boldsymbol{H}_1 = \begin{bmatrix} 0&0&0&0&0\\0&0&0&0&0\\0&0&0&0&0\\0&0&0&0&0\\0&0&0&0&0 \end{bmatrix}; \quad \boldsymbol{H}_2 = \begin{bmatrix} 0&0&0&0&0\\0&0&0&0&0\\0&0&0&0&0\\0&0&0&0&0\\0&0&0&0&0 \end{bmatrix}; $$

$$ \boldsymbol{H}_3 = \begin{bmatrix} 0&0&0&0&0\\0&0&0&0&0\\0&0&0&0&0\\0&0&0&0&0\\0&0&0&0&0 \end{bmatrix}; \quad \boldsymbol{H}_4 = \begin{bmatrix} 0&0&0&0&0\\0&0&0&0&0\\0&0&0&0&0\\0&0&0&0&-\mathrm{s}\alpha\\0&0&0&0&0 \end{bmatrix}; $$

$$ \boldsymbol{H}_5 = \begin{bmatrix} 0&0&0&0&0\\0&0&0&0&0\\0&0&0&0&0\\0&0&0&0&0\\0&0&0&0&0 \end{bmatrix}; \quad \boldsymbol{H}_6 = \begin{bmatrix} 0&0&0&0&0\\0&0&0&0&0\\0&0&0&0&0\\0&0&0&0&0\\0&0&0&0&\mathrm{c}\alpha \end{bmatrix}. $$

When $\dot{\boldsymbol{X}}$ and $\ddot{\boldsymbol{X}}$ are known, the acceleration of 5-SPS limbs in (5-SPS)+5R2U HRDM can be obtained by Eq. (26)~Eq. (33).

4. Factors affecting workspace

Workspace is the active area which can be reached by the reference point of the moving platform, which is one of the important indexes to measure the kinematic performance of the mechanism. The activity space of HRDM is the public area that can be reached by the reference point of the moving platform under the joint action of each limb. It is the intersection of the workspace generated by 5-SPS limbs and the HRDL in the center of the moving platform.

4.1. Factors affecting the workspace of 5-SPS PM

The main factors affecting the workspace of 5-SPS limbs are the activity of spherical pairs the length of the spherical pairs and the interference range of the spherical pairs. Expressed as the following mathematical relationship:

$$ W_R = \begin{cases} -\sigma_{max} \le \sigma_i \le \sigma_{max}, & i = 1, 2, \ldots, 5 \\ L_{min} \le L_j \le L_{max}, & j = 1, 2, \ldots, 5, \\ d_{i,j} \ge d_{\min}, & i \ne j \end{cases} \tag{34} $$

where: σ_i is the activity of the i_th spherical pairs, and σ_{max} is the limit value of the spherical pairs activity space; σ_i is the length of the j_th driving rod, and l_{min} and l_{max} are the limit values of the length of prismatic pairs; $d_{i,j}$ is the distance between links and d_{min} is the limit distance between links.

4.2. Factors affecting HRDL workspace

1. Parameters of planar five bar mechanism.

The workspace of 5-SPS limbs of HRDM is determined, and HRDL restricts the movement of the whole mechanism. It is composed of parallel / series mechanisms, and its workspace is determined by the planar PM CDEFG and the spatial connecting rod EO'. Reachable interval workspace and reachable space point set of coupling point E, and the constraint condition is:

$$ \begin{cases} |l_1 - l_2| < l_e < l_1 + l_2 \\ |l_3 - l_4| < l_e < l_3 + l_4 \end{cases}. \tag{35} $$

2. Constraint of spatial link.

The upper and lower limit values of the center track of the moving platform of HRDL are within the maximum and minimum driving range of the 5-SPS prismatic pairs. l_{min} and l_{max} are the minimum and maximum travel of 5-SPS limbs prismatic pair respectively, thus the maximum movement area of 5-SPS limbs in Y_1 direction is:

$$ \begin{cases} y'_{\min} = \sqrt{(l + l_{\min})^2 - (R - r)^2} \\ y'_{\max} = \sqrt{(l + l_{\max})^2 - (R - r)^2} \end{cases} (i = 1, 2, ..., 5). \tag{36} $$

The reachable workspace of HRDL is $X' = (x', y', z')$, which satisfies the following constraints:

$$ f(X') = (x' - x_e)^2 + (y' - y_e)^2 + z'^2 - l_7^2. \tag{37} $$

The workspace of HRDM is the intersection of HRDL and 5-SPS limbs. If there is a common area between the two, HRDL must meet the operation interval of y' in Y_1 direction of 5-SPS limbs determined by constraint Eq. (37) $\varphi(X') = 0$ (the interval determined by Eq. (36)), i.e.

$$ y' \in [\varphi(X') = 0], \; x', z' \in X. \tag{38} $$

If there is intersection between HRDL and 5-SPS limb, the conditions must be met:

$$y'_{min} \le y' \le y'_{max}. \tag{39}$$

The workspace of the whole mechanism should be determined jointly according to the position and orientation of the mechanism and the structure parameters of the all sub-limbs.

5. Workspace atlas of (5-SPS)+5R2U

The workspace of (5-SPS)+5R2U HRDM is jointly determined by 5-SPS limbs and HRDL, which is the intersection of the two workspaces.

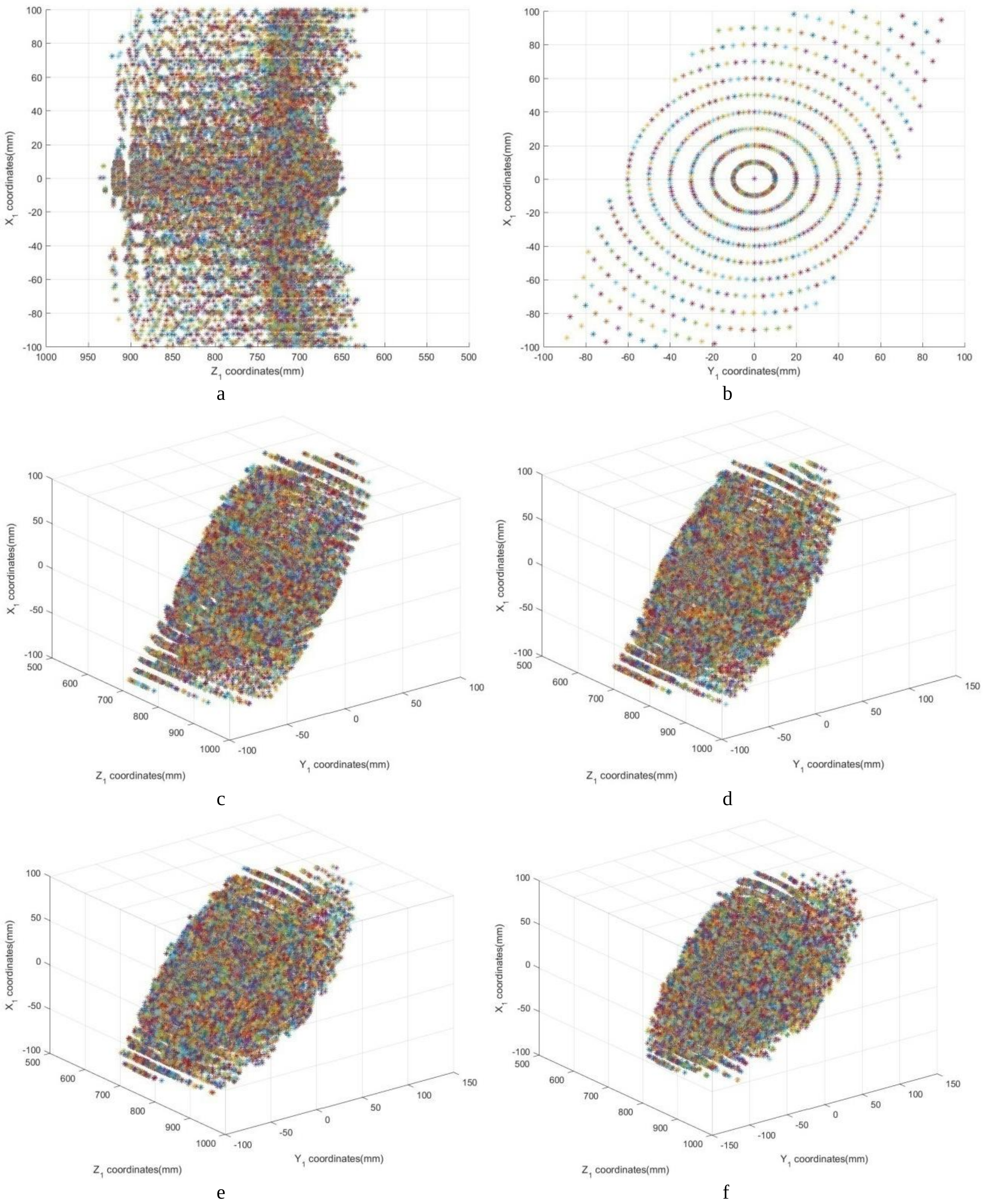

Fig. 6 Workspace atlas under different angles α: a) projection of the workspace on the $X_1O_1Z_1$ plane when $\alpha = 0°$; b) projection of the workspace on the $X_1O_1Y_1$ plane when $\alpha = 0°$; c) 3D diagram of workspace when $\alpha = 0°$; d) 3D diagram of workspace when $\alpha = 5°$; e) 3D diagram of workspace when $\alpha = 10°$; f) 3D diagram of workspace when $\alpha = 15°$; g) 3D diagram of workspace when $\alpha = 20°$; h) 3D diagram of workspace when $\alpha = 25°$

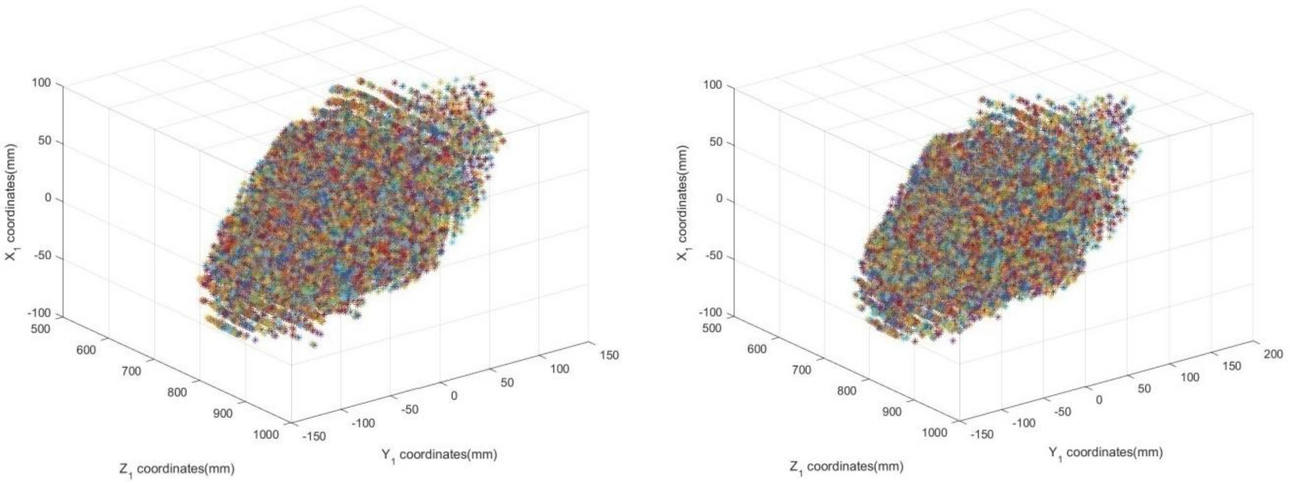

g h

Fig. 6 Continuation

Define the driving range of prismatic pairs of 5-SPS limbs as (0~400 mm), and the maximum swing angle of spherical pair is 45°, and the maximum rotation angle of Hooke hinge is 60°. From Eq. (34) to Eq. (39), the constraint conditions and kinematic Eq. (10) and Eq. (17) of HRDM workspace are affected, and the workspace atlas under different flexible orientation angles are obtained, as shown in Fig. 6.

As can be seen from Fig. 5, the workspace atlas of (5-SPS)+5R2U HRDM presents the following characteristics:

1. When the flexible orientation angle of the mechanism $\alpha = 0°$, the mechanism is translational. At this time, the *U* plane of the *U* pair in the HRDL constraint limb always remains parallel, that is, the motion of the constraint of the 5R2U constraint limb is the rotation of the moving platform around its normal, which does not affect the workspace of the mechanism. Therefore, the workspace of the mechanism is the same as that of the 5-SPS mechanism. The maximum movement range (650~950) mm of the mechanism in X_1 direction is similar to the cylinder at a certain angle to the coordinate plane $X_1O_1Y_1$ and the workspace is symmetrical about Y_1 axis.

2. When the flexible orientation angle of the mechanism α is gradually increasing, the workspace of the mechanism gradually increases in x_1 direction and decreases in z_1 direction. Because the intermediate constraint limb 5R2U is composed of parallel/series mechanisms, the workspace of the planar five-bar mechanism is the intersection of several rings, which has a great impact on the scope of the workspace.

6. Kinematic example of HRDM

Set the angular velocity of the CV motor as $\dot{q}_1 = 30°/\text{s}$, and it takes 12 s for the CV motor to run for a cycle. The motion law of the center point of the moving platform of the mechanism is defined as:

$$\begin{cases} x = 20sin\left(\pi t / 6\right) \\ y = 20cos\left(\pi t / 6\right) \\ z = 0.2t \\ \alpha = 0 \\ \gamma = 0 \end{cases} \qquad (0 \le t \le 12). \tag{41}$$

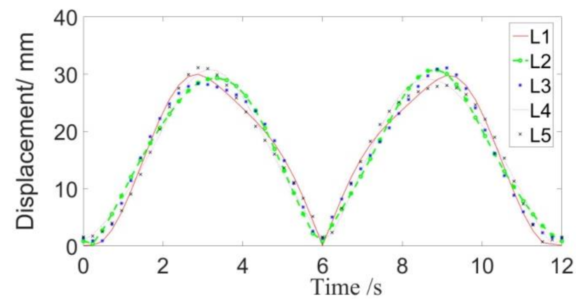

Fig. 7 Variations of the displacement $l_i(i = 1, 2,…,5)$ in 5-SPS limbs

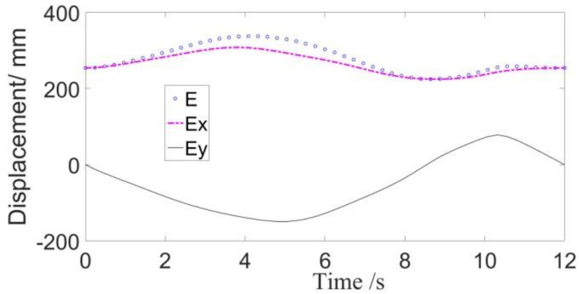

Fig. 8 Variations of the displacement of point E

According to the inverse solution Eq. (17) of HRDM, the variation law of the displacement $l_i(i = 1, 2,…,5)$ in 5-SPS limbs are obtained, as shown in Fig. 7. The position of point *E* of HRDL is shown in Fig. 8, and the variation law of the angular displacement of $\boldsymbol{q}_i(i = 1, 2,…,5)$ is shown in Fig. 9. The driving variation laws of the driving velocity of 5-SPS limbs are obtained from Eq. (27), as shown in Fig. 10.

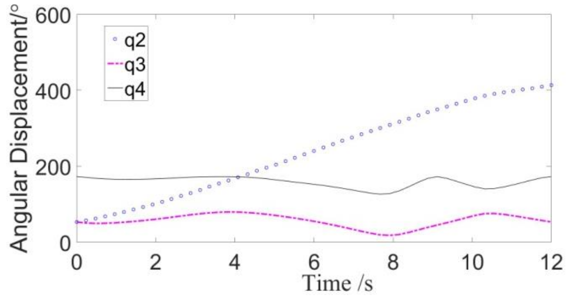

Fig. 9 Variation law of the angular displacement $q_i(i = 1, 2, 3, 4)$

The variation of the velocities of point *E* is shown in Fig. 11; The variation laws of the compensation angular velocity $\dot{q}_4$ of HRDL servo motor and angular velocity $\dot{q}_2$, and $\dot{q}_3$ of included angle of links is shown in Fig. 12. The acceleration variation laws of 5-SPS limbs are shown in Fig. 13. The variation laws of the acceleration of the coupling point *E* are shown in Fig. 14.

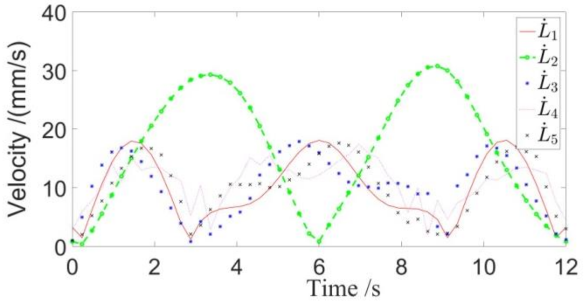

Fig. 10 Variation law of velocity of 5-SPS driving sliders

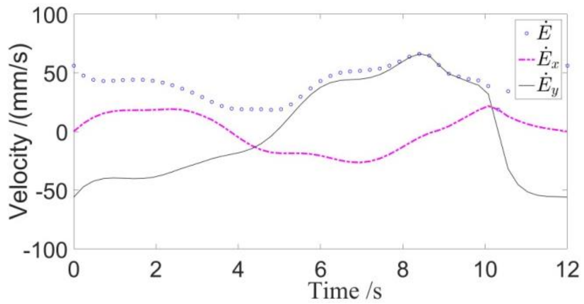

Fig. 11 Variation law of the velocity point *E*

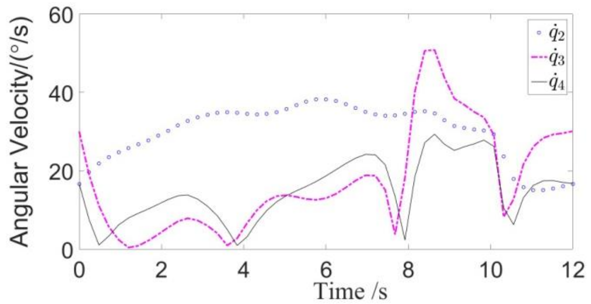

Fig. 12 Variation law of the angular velocity $\dot{q}_i\left(i=2,3,4\right)$

The midpoint trajectory ***X*** of the planned moving platform is coherent and smooth. By analyzing the variation laws of the curves in Figs. (7)~(15), the following conclusions can be drawn.

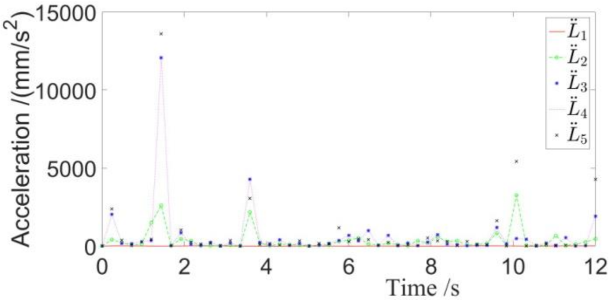

Fig. 13 Acceleration variation curves of 5-SPS

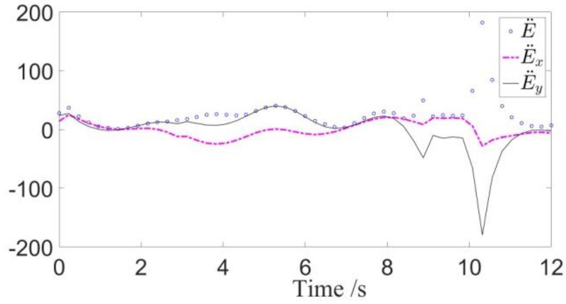

Fig. 14 Variation law of the acceleration of point *E*

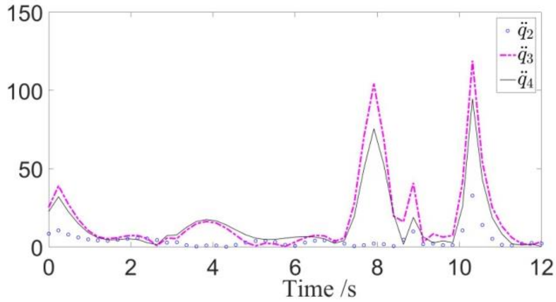

Fig. 15 Variation law of the angular acceleration $\ddot{q}\left(i=2,3,4\right)$

1. The inverse solutions $l_i(i$ = 1, 2,…,5) and $q_i(i$ = 1, 2, 3, 4) of the HRDM driving limb are unique with the determination of the driving angular displacement q4 of the HRDL servo motor.

2. The virtual limb $\boldsymbol{l}_v$ inverse solution is uniquely determined, and the displacement curve is smooth and continuous without jump. The velocity variation range is between (-60~70) mm/s, and the impulse generated by the moving platform is very small. Most of the variation areas of acceleration are (-200~200) mm/s. Thus, the variation range is small and the impact force on the moving platform is small.

3. The variation curves of the displacement l_i and the velocity $\dot{l}_i$ of the driving limb 5-SPS, the variation curves of the angular displacement q_4 and angular velocity $\dot{q}_4$ driven by the servo motor are all smooth and coherent. At the same time, the variation curves of the driving acceleration $\ddot{h}_i$ and angular acceleration $\ddot{q}_4$ are all smooth without jump and sudden change, which ensures the stability of the mechanism operation and the overall controllability of the mechanism.

4. Servo motor q_4 is a regulating motor, and its velocity variation range is (0~50) °/s. When making the planned trajectory movement, the rotating torque is small and will not damage the motor shaft. $\ddot{\boldsymbol{q}}_2$ changes greatly in (7~9) s and $\ddot{\boldsymbol{q}}_3$ in (10~11) s, but the variation range is between (0~130) °/s, and the impact is limited. The mechanism can still operate smoothly.

7. Conclusion

The spatial 5-DOF HRDM takes the CV motor as a drive of the redundantly actuated PM, organically combines the hybrid-driven theory and the redundantly actuated mechanism, and constructs a new mechanism. It successfully extends the hybrid-driven theory to the spatial mechanism and widens the research field of the hybrid-driven mechanism. Taking (5-SPS)+5R2U mechanism as an example, kinematics is analyzed, and the following conclusions are drawn:

1. In the HRDM, the HRDL not only restricts the DOFs of the whole mechanism, but also a limb controlled by the CV motor and servo motor. The CV motor provides the main power, and the servo motor accurately compensates the trajectory of the moving platform. This mechanism can be extended to a spatial mechanism with n (n = 3, 4, 5, 6) DOFs.

2. The position equation of the HRDM is established by using the vector method, and the inverse solution equation and the analytical equations of velocity and acceleration are obtained. The inverse Jacobian matrix is expressed as the explicit functional relationship between motion input and motion output. The form is simple and convenient for real-time control.

3. Through the analysis of workspace and kinematics simulation, the inverse solution of mechanism is unique with the determination of initial configuration. It is obtained that the motion trajectory of the mechanism is continuous and smooth in space, and is real-time controllable in workspace.

Acknowledgments

This work was supported by the Key Research and Development Program of Shanxi Province of China (International Cooperation, Nos. 201803D421027, 201903D421051, 2022ZDYF082), the Opening Foundation of Shanxi Key Laboratory of Advanced Manufacturing Technology (Grant Nos. XJZZ201807, XJZZ202302) and the Natural Science Foundation of Shanxi Province, China (Grant No. 201701D121079).

References

1. **Tokuz, L. C.** 1992. Hybrid Machine Modelling and Control, Ph.D. thesis, Liverpool Polytechnic, UK.
2. **Li, R. Q.; Wang, Y.; Wang, M. Y.; Zhao, Y. H.; Song, J.** 2016. Research progress and development trend of hybrid-driven mechanism, Journal of Mechanical Engineering 52(13): 1-9 (in Chinese). https://doi.org/10.3901/JME.2016.13.001.
3. **Zi, B.; Cao, J.B.; Zhu, Z.C.** 2011. Dynamic simulation of hybrid-driven planar five-bar parallel mechanism based on simMechanics and tracking control, International Journal of Advanced Robotic Systems 8(4): 28-33. https://doi.org/10.5772/45683.
4. **Soong, R.** 2015. On the hybrid-driven linkage mechanism with one input cycle corresponding to two output cycles, Transactions of the Canadian Society for Mechanical Engineering 39(3): 637-646. https://doi.org/10.1139/tcsme-2015-0050.
5. **Guo, W. Z.; He, K.; Yeung, K.; Du, R.** 2005. A new type of controllable mechanical press: Motion control and experiment validation, Journal of Manufacturing Science and Engineering 127(4): 731–742. https://doi.org/10.1115/1.1954791.
6. **Li, C.; Tso, P.** 2008. Experimental study on a hybrid-driven servo press using iterative learning control, International Journal of Machine Tools and Manufacture 48(2): 209-219. https://doi.org/10.1016/j.ijmachtools.2007.08.01.
7. **Li, H.; Fu, L. H.; Zhang, Y. P.** 2010. Optimum design of a hybrid-driven mechanical press based on inverse kinematics, Journal of Mechanical Engineering 56(5): 301-306 (in Chinese).
8. **Tso, P.** 2010. Optimal design of a hybrid-driven servo press and experimental verification, Journal of Mechanical Design 132(3): 1-4. https://doi.org/10.1115/1.4000213.
9. **Chen, X. L.; Tang, Y. F.; Gao, S.** 2022.Dynamic modeling and analysis of hybrid driven multi-link press mechanism considering non-uniform wear clearance of revolute joints, Meccanica 57(1): 229-250 https://doi.org/10.1007/s11012-021-01453-w.
10. **Wang, Z. R.; Dong, E. B.; Xu, M.; Yang, J.** 2015. Circling turning loco-motion of a new multiple closed-chain-legs robot with hybrid-driven mechanism, Advanced Robotics 29(24):1637-1648. http://dx.doi.org/10.1080/01691864.2015.1071682.
11. **Zhu, K. J; Cai, G. W.; Zhang, L.; Chen, Y.; Tang, J. B.** 2016. Kinematic analysis and working space numerical solution of a novel three degree of multi-link hybrid-driven mechanism, Heavy Machinery (5): 61-67 (in Chinese). http://dx.doi.org/10.13551/j.cnki.zxjxqk.2016.05.013.
12. **Kong, X. W.; Gosselin, C.** 2005.Type synthesis of 5-DOF parallel manipulators based on screw theory, Journal of Robotic Systems 22(10): 535-547. http://dx.doi.org/10.1002/rob.20084.
13. **Piccin, O.; Bayle, B.; Maurin, B.; Mathelin, M.** 2009. Kinematic modeling of a 5-DOF parallel mechanism for semispherical workspace, Mechanism and Machine Theory 44(8): 1485-1496. http://dx.doi.org/10.1016/j.mechmachtheory.2008.11.012.
14. **Gao, F.; Peng, B. B.; Zhao, H.; Li, W. M.** 2006. A novel 5-DOF fully parallel kinematic machine tool, The International Journal of Advanced Manufacturing Technology 31:201-207. http://dx.doi.org/10.1007/s00170-005-0171-1.
15. **Kanaan, D.; Wenger, P.; Chablat, D.** 2009. Kinematic analysis of a serial–parallel machine tool: The VERNE machine, Mechanism and Machine Theory 44(2): 487-498. https://doi.org/10.1016/j.mechmachtheory.2008.03.002.
16. **Ebrahimi, I.; Carretero, J.; Boudreau, R.** 2007. 3-PRRR redundant planar parallel manipulator: Inverse displacement, workspace and singularity analyses, Mechanism and Machine Theory 42(8): 1007-1016. https://doi.org/10.1016/j.mechmachtheory.2006.07.006.
17. **Wu, J.; Zhang, B. B.; Wang, L. P.** 2016. Optimum design and performance comparison of a redundantly actuated solar tracker and its non-redundant counterpart, Solar Energy 127: 36-47. http://dx.doi.org/10.1016/j.solener.2016.01.017.
18. **Lambert, P.; Herder, J. L.** 2019. A 7-DOF redundantly actuated parallel haptic device combining 6-DOF manipulation and 1-DOF grasping, Mechanism and Machine Theory 134: 349-364. https://doi.org/10.1016/j.mechmachtheory.2019.01.002.
19. **Zhang, H. Q.; Fang, H. R.; Zhang, D.; Luo, X. L.;**

Zou, Q. 2019. Forward kinematics and workspace determination of a novel redundantly actuated parallel manipulator, International Journal of Aerospace Engineering 2019: 1-14.
https://doi.org/10.1155/2019/4769174.
20. **Wang, C. Z.; Fang, Y. F.; Guo, S.; Zhou, C. C.** 2015. Design and kinematic analysis of redundantly actuated parallel mechanisms for ankle rehabilitation, Robotica 33(2): 366–384.
https://doi.org/10.1017/S0263574714000241.
21. **Zhao, Y. J.; Gao, F.; Li, W.; Liu, W.; Zhao, C.** 2009. Development of 6-dof parallel seismic simulator with novel redundant actuation, Mechatronics: The Science of Intelligent Machines 19(3): 22-427.
https://doi.org/10.1016/j.mechatronics.2008.11.013.
22. **Zhang, Q. S.; LI, R. Q.; Liang, J. J.** 2019. Kinematics and controllability analysis of n-DOF hybrid redundantly driven mechanism, Science Technology and Engineering, 19(20): 196-202 (in Chinese).
23. **Zhang, Q. S.; Li, R. Q.; Liang, J. J.** 2022. Kinematics and workspace atlas of 3-PSS/7R hybrid redundantly driven mechanism, Mechanics 28(1): 73-81.
http://dx.doi.org/10.5755/j02.mech.28987.

Q. Zhang, R. Li, W. Yao, J. Liang, F. Ning

KINEMATICS AND WORKSPACE ANALYSIS OF 5-DOF HYBRID REDUNDANTLY DRIVEN MECHANISM

S u m m a r y

A novel 5-DOF (5-SPS)+5R2U hybrid redundantly driven mechanism (HRDM for short) is proposed, which can realize 3 translations and 2 rotations (3T2R) movements. (5-SPS)+5R2U parallel mechanism is composed of six driving limbs. Of which 5-SPS (S represents spherical pair, P represents prismatic pair) limbs are symmetrically distributed at the center point of static and moving platform have no restriction on the degrees of freedom of the mechanism. The middle limb (7R)U (R represents revolute pair, U represents Hooke joint) is connected to the static platform and the center point of the moving platform. It is jointly driven by constant velocity motor and servo motor, and plays a role of restraining the freedom of the whole mechanism. It is called hybrid redundantly driven limb (HRDL for short). Hybrid-driven mechanism and redundantly actuated mechanism can be integrated into one mechanism by HRDL, which can give full play to the advantages of both. The inverse position solution model of the mechanism is established, and the velocity Jacobian matrix and acceleration expression are derived to obtain the velocity and acceleration variation laws of the mechanism. On this basis, the factors affecting the workspace are analyzed, and the workspace atlas under different orientation angles is obtained. The results provide theoretical model for the realization planning trajectory of (5-SPS)+5R2U HRDM.

Keywords: (5-SPS)+5R2U parallel mechanism, hybrid redundantly driven, Jacobian matrix, kinematic analysis, workspace.

Received March 9, 2023
Accepted December 3, 2023